EBSA
Biophysics in Europe

Check for updates

Determination of mRNA copy number in degradable lipid nanoparticles via density contrast analytical ultracentrifugation

Alexander Bepperling[1] [ORCID] · Gesa Richter[1]

Abstract

Lipid nanoparticles as delivery system for mRNA have recently attracted attention to a broader audience as COVID-19 mRNA vaccines. Their low immunogenicity and capability to deliver a variety of nucleic acids renders them an interesting and complementary alternative to gene therapy vectors like AAVs. An important quality attribute of LNPs is the copy number of the encapsulated cargo molecule. This work describes how density and molecular weight distributions obtained by density contrast sedimentation velocity can be used to calculate the mRNA copy number of a degradable lipid nanoparticle formulation. The determined average copy number of 5 mRNA molecules per LNP is consistent with the previous studies using other biophysical techniques, such as single particle imaging microscopy and multi-laser cylindrical illumination confocal spectroscopy (CICS).

Introduction

Since their initial description, lipid nanoparticles (LNPs) have made a remarkable career as delivery tools for drugs to human cells. From simple liposomes (Bangham et al. 1965) over the first cationic mRNA–LNP formulation (Malone et al. 1989), flu vaccines, and drug carriers, they finally became popular to a broader audience as COVID-19 mRNA vaccines (Ramachandran et al. 2022).

Today, the LNP-mediated therapeutic transfer of nucleic acids centers around siRNAs and mRNAs with over 200 products in clinical trials (Tenchov et al. 2021), while antisense-oligonucleotides (ASO) and GalNAc−siRNA conjugates are often injected as pure substance without an additional delivery system. The immunogenicity and toxicity of free mRNA as well as its instability prevents this administration route for native and chemically modified mRNA.

To function in human body systems as a drug, mRNA formulations need to resist biophysical and biochemical barriers. In pure form, thus without a delivery system, mRNA is exposed to ribonuclease (RNase) degradation, renal clearance and immune detection and reaction (Yin et al. 2014). Delivery systems like mRNA packed in LNPs can overcome those barriers and additionally reach target tissue, promote endocytotic cell entry, and cross cell membranes.

Beside the advantages of the LNPs, any potential toxicity issues must be intensively studied. Toxicity in LNPs has been previously shown to depend on both the particle composition and the nanoparticle size (Bobo et al. 2016). Nanoparticle toxicity is often associated with the production of reactive oxygen species (ROS) (Xia et al. 2006). Additionally, interactions with cellular components such as the nucleus can be associated with increased toxicity (Marquis et al. 2009). Especially in cationic lipid containing formulations toxicity is a relevant topic, as those lipids are synthetic and their effect on the human body may not always be known. It has been shown that increased delivery effectiveness of cationic lipids is linked to increased toxicity (Tenchov et al. 2021). To minimize those toxic effects, efforts are made to develop efficient models of biodegradable LNPs. The toxicity and immunogenicity of free mRNA mandates a rigorous characterization of the final product regarding mRNA loading ratio and the absence of free mRNA.

✉ Alexander Bepperling
alexander.bepperling@novartis.com

[1] Novartis TRD, Keltenring 1+3, 82041 Oberhaching, Germany

Analytical Ultracentrifugation (AUC) is exquisitely suited to fulfill this role as the rotor speed can be freely adjusted to cover a size range from 1 kDa peptides up to GDa protein complexes (or some 100 nm, respectively). The advent of new instrumentation and detection systems fostered the development multiwavelength experiments (Gorbet et al. 2015; Walter et al. 2015; Horne et al. 2020; Henrickson et al. 2021, 2022; Maruno et al. 2021, 2022; McIntosh et al. 2021; Hayes and Dobnik 2022)which have proven their great potential for the analysis of gene therapy products.

LNPs are inherently heterogeneous and complex products but also offer an additional dimension of separation by AUC. Delivery system (lipids) and cargo (RNA) have vastly different densities which influence their sedimentation behavior. This can be further exploited by density variation experiments in the presence of different D_2O or other water isotope concentrations. This method has been recently developed by Henrickson et al. (Henrickson et al. 2021) and was used to investigate the loading ratio of different siRNA formulations.

Here, we demonstrate how such a density distribution can be deconvoluted into the fraction of lipid and mRNA, and subsequently, the number of mRNA copies per capsid be calculated.

Materials and methods

Materials

Empty DLPs and DLPs containing an 1156-nucleotide long mRNA cargo (DLP-1156) were provided by the Novartis Institute for Biomedical Research (NIBR), Cambridge

(MA). A scheme of its assembly including the nucleic acid cargo is given in Fig. 1. Lipid nanoparticles were prepared by spontaneous mixing through a "T" microfluidic apparatus as previously described (Wilson et al. 2015). The four lipids were dissolved in ethanol at the ratio given in Fig. 1. The mRNA was prepared in 100 mM sodium chloride and 20 mM sodium citrate at pH 5. Both solutions were mixed to obtain a molar ratio of amine groups on ionizable lipids to phosphate groups on mRNA (N/P ratio) of 4.5 using the "T" microfluidic apparatus. The obtained solution was further diluted with citrate buffer and subsequently rebuffered in PBS by tangential flow filtration.

Dulbecco's phosphate-buffered saline (PBS, powder, and liquid) was purchased from Gibco. PBS in D_2O was prepared by dissolving the respective amount of PBS powder in D_2O (99.9%, Sigma-Aldrich).
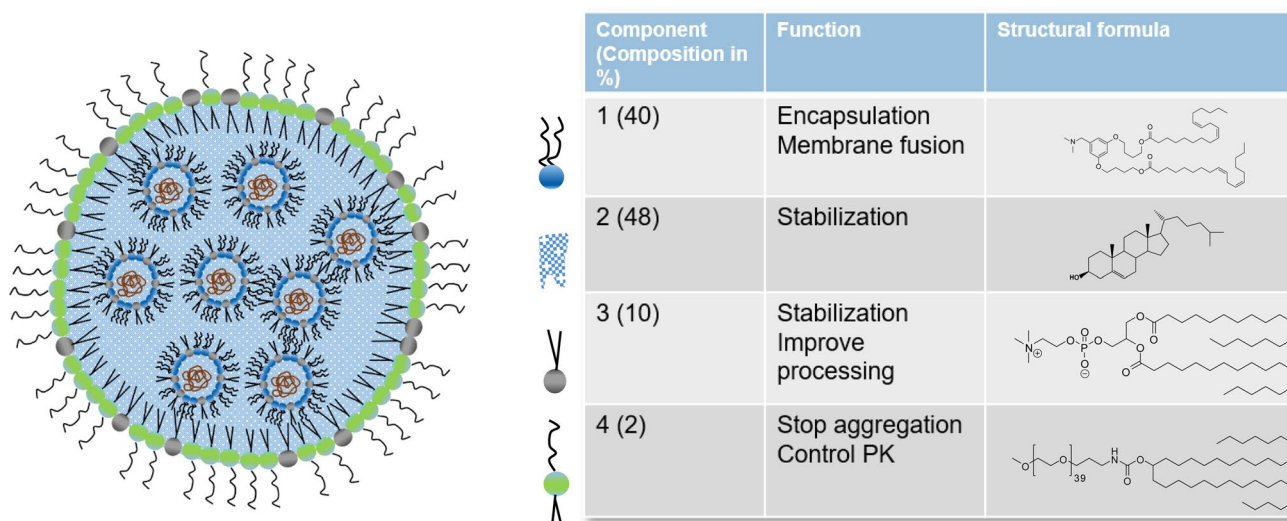
Photometric measurements

UV-spectra of the undiluted DLP and DLP-1156 samples were recorded from 200 to 800 nm using an Implen NP80 nanodrop UV spectrophotometer.

Experimental procedure and data analysis AUC.

Sedimentation velocity AUC

Analytical ultracentrifugation was performed with an Optima AUC analytical ultracentrifuge (Beckman, Krefeld, Germany) supplied with absorbance and interference optics. 480 μL of sample and 480 μL PBS as reference (for interference measurements) were loaded into assembled cells with sapphire windows and 12-mm path length

Component (Composition in %)	Function	Structural formula
1 (40)	Encapsulation Membrane fusion	
2 (48)	Stabilization	
3 (10)	Stabilization Improve processing	
4 (2)	Stop aggregation Control PK	

Fig. 1 Scheme of LNP assembly including nucleic acid cargo and function of the four lipids (1 = cationic lipid, 2 = cholesterol, 3 = neutral lipid, 4 = PEG shielding lipid)

charcoal-filled epon double sector centerpieces (CP). The samples were analyzed at 20,000 rpm or 14,000 rpm in an eight-hole Beckmann-Coulter AN50-Ti rotor. Sedimentation was monitored at 260 nm continuously scanned with a radial resolution of 10 microns taking one replicate per time point. Data analysis was carried out using the software UltraScan 4 (Demeler and Gorbet 2016). Intensity data were subjected to 2DSA analysis (custom grid) with meniscus and iterative fitting followed by PCSA with 100 Monte-Carlo iterations. All UltraScan calculations were done in-house on a Ryzen128-1019 Gigabyte TRX40 AORUS PRO with an AMD Ryzen Threadripper 3990X 2.9 GHz 64 Core/128 Threads CPU.

Density-matching sedimentation velocity

The data acquisition and analysis followed the procedure developed and described by Henrickson et al. (Henrickson et al. 2021). In brief, DLP and DLP-1156 were diluted with PBS supplemented with D_2O (concentrations see Figs. 2 and 3) to an OD260 of 0.8. The samples were loaded into standard 12-mm CP AUC cells and inserted into an An-50 Ti rotor equilibrated at 20 °C. The rotor speed was set to 20,000 rpm and data were recorded at 260 nm for 5 h. All datasets were fitted to the 2DSA-IT stage and imported into the "density matching" module of Ultrascan. Until this point, the data had only been corrected to the viscosity of the respective D_2O concentrations using Sednterp 3.0 (Laue et al. 1992; Hayes et al. 2000; Philo 2023) but not for the density which takes place in the "density matching" module of Ultrascan.
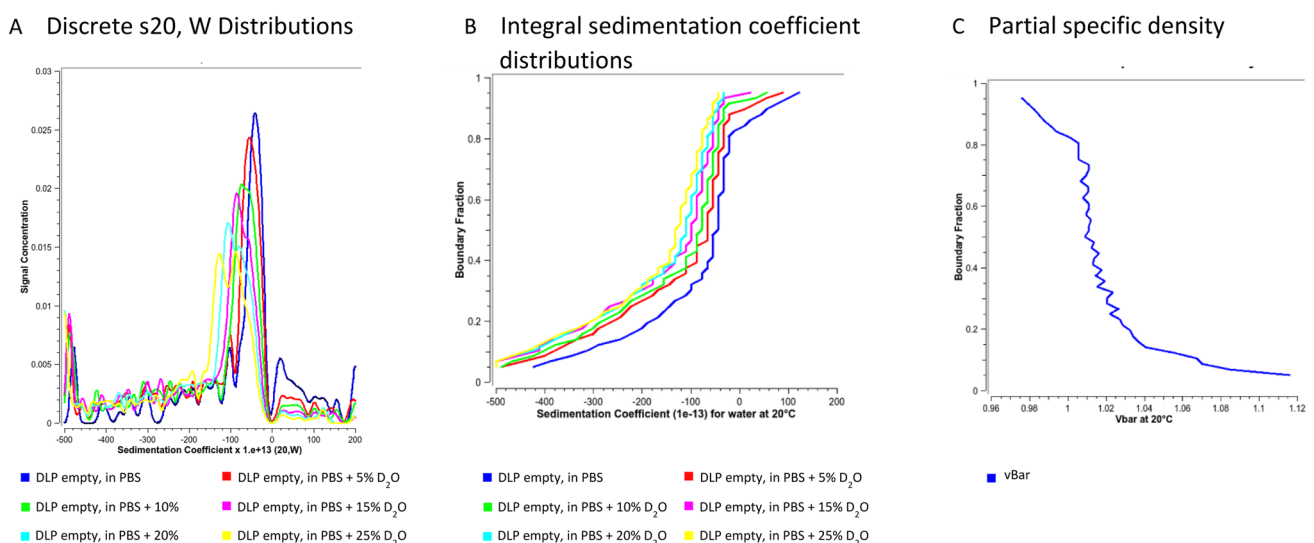
Multi-wavelength SV-AUC

DLP and DLP-1156 were diluted using PBS to an OD280 of 0.8 and loaded into one standard 12-mm CP AUC cell. The rotor speed was set to 14,000 rpm and data from 31 wavelengths (230–290 nm in 2 nm steps) were recorded. All 31 datasets were fitted to the 2DSA-IT stage and simulated to a synchronous time grid.
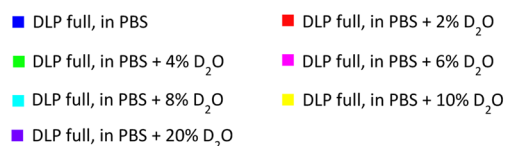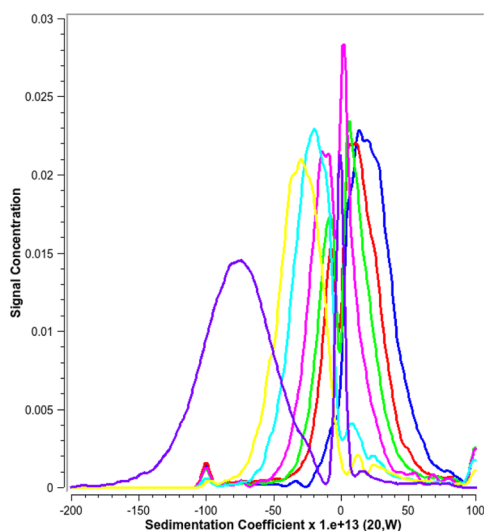
Results and discussion

First, we determined the partial specific volume of the empty LNPs, which are composed of 45% Cationic lipid, 44% Cholesterol, 9% neutral lipid (DSPC = 1,2-distearoyl-sn-glycero-3-phosphocholine), and 2% of shielding lipid (PEG-lipid) (Fig. 1).

Figure 2 shows the sedimentation coefficient distribution of the empty DLPs in PBS supplied with 0–25% D_2O and the derived partial specific volume distribution. A small fraction of the material is sedimenting toward the bottom of the cell but most of it floats with a vbar up to 1.12 cm^3/g centered around a main fraction with a vbar of 1.014 cm^3/g.
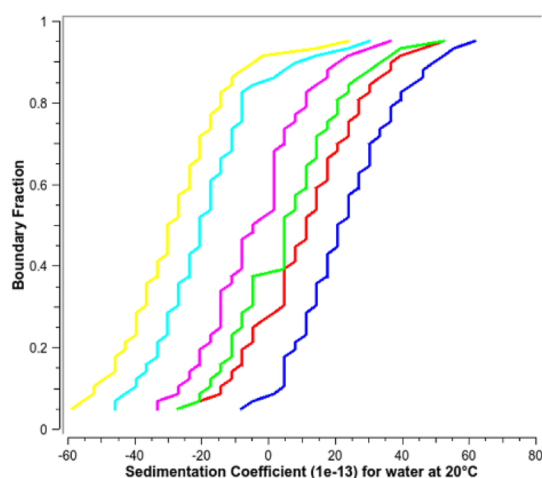
The loaded LNPs (LNP-1156) contained about 7% of floating material. A first density contrast experiment using up to 90% D_2O caused the particles to fully float at already 20% D_2O shortly after the start of the experiment (Fig. S4). We therefore chose to probe a D_2O concentration space of 2–20% (Fig. 3A). At a D_2O concentration of 4%, about half of the material sedimented, while the other half floated. As a sedimentation coefficient of zero is not possible in the Lamm
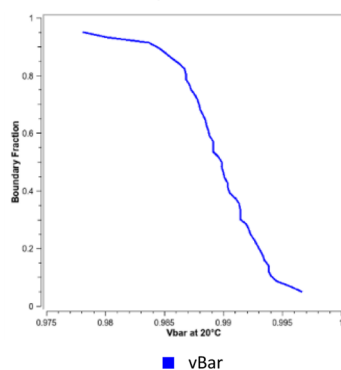

A Discrete s20, W Distributions

B Integral sedimentation coefficient distributions

C Partial specific density

- DLP empty, in PBS
- DLP empty, in PBS + 5% D_2O
- DLP empty, in PBS + 10%
- DLP empty, in PBS + 15% D_2O
- DLP empty, in PBS + 20%
- DLP empty, in PBS + 25% D_2O

- DLP empty, in PBS
- DLP empty, in PBS + 5% D_2O
- DLP empty, in PBS + 10% D_2O
- DLP empty, in PBS + 15% D_2O
- DLP empty, in PBS + 20% D_2O
- DLP empty, in PBS + 25% D_2O

- vBar

Fig. 2 **A** Overlay of sedimentation coefficient distributions of empty LNPs in PBS supplied with 5–25% D_2O. Dataset was analyzed using UltraScan. **B** Integral sedimentation coefficient distributions of (**A**). **C** Partial specific density shown by vbar plotted versus boundary fraction
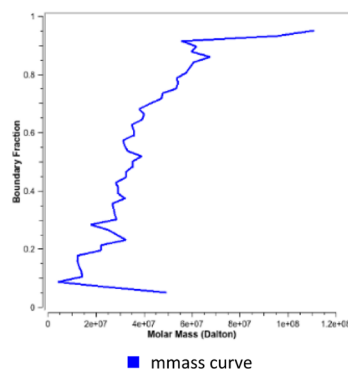
A Discrete s20, W Distributions

B Integral sedimentation coefficient distributions

Legend A:
- DLP full, in PBS
- DLP full, in PBS + 2% D_2O
- DLP full, in PBS + 4% D_2O
- DLP full, in PBS + 6% D_2O
- DLP full, in PBS + 8% D_2O
- DLP full, in PBS + 10% D_2O
- DLP full, in PBS + 20% D_2O

Legend B:
- DLP full, in PBS
- DLP full, in PBS + 5% D_2O
- DLP full, in PBS + 10% D_2O
- DLP full, in PBS + 15% D_2O
- DLP full, in PBS + 20% D_2O
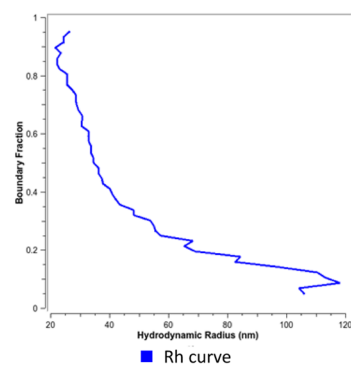- DLP full, in PBS + 25% D_2O

C Partial specific density

D Molar mass

E Hydrodynamic radius

Fig. 3 **A** Overlay of sedimentation coefficient distributions of loaded LNPs (LNP-1156) in PBS supplied with 2–20% D_2O. Dataset was analyzed using UltraScan. **B** Integral sedimentation coefficient distributions of loaded LNPs (LNP-1156) in PBS supplied with 2–10% D_2O. **C** Partial specific density shown by vbar plotted versus boundary fraction. **D** Molar mass plotted versus boundary fraction. **E** Hydrodynamic radius shown by Rh curve plotted versus boundary fraction

equation, all distributions crossing that point will show a "dip" at zero.

We analyzed the six sedimentation coefficient distributions from 0 to 10% of the full particles with the density matching module of Ultrascan (Fig. 3B). Based on these sedimentation coefficient distributions and their corresponding D_2O concentrations, the software calculates a vbar (Fig. 3C), a molar mass (Fig. 3D), and a hydrodynamic radius (Fig. 3E) distribution for $D_2O = 0$.

The resulting partial specific volume distribution is rather continuous (Fig. 3C) than being centered around a

main species like that of the empty particles. It ranges from 0.978 cm^3/g to 0.996 cm^3/g with a midpoint (boundary fraction = 0.5) of 0.990 cm^3/g, which is identical to the vbar used to analyze SV-AUC data of an mRNA vaccine (Comirnaty) during a stability study (Thaller et al. 2023). At this point, the data already reveal that the LNP-1156 preparation contains very little-to-almost no empty LNPs and that the loaded particles consist mainly of lipid as the vbar is smaller than 1.0 cm^3/g but very close that of the empty vectors (1.014 cm^3/g) and far away from the vbar of nucleic acids in low-salt buffers. We used a vbar of 0.53 cm^3/g for the

mRNA in PBS (Enger et al. 1963; Funari et al. 2000; Voss and Gerstein 2005; Padlan et al. 2014) assuming a similar composition (ionic strength) of the aqueous phase inside the LNPs. The vbar distribution of the loaded particles can be deconvoluted into the relative fraction of RNA and lipid by the following equation:

$$[\%]_{(lipid)} = \left[vbar_{(full\ LNP)} - vbar_{(RNA)} / vbar_{(lipid)} - vbar_{(RNA)} \right] * 100 \tag{1}$$

where "$vbar_{(full\ LNP)}$" represents each point of the vbar distribution of the loaded particles. Inserting, for example, the value from the midpoint of the vbar distribution (boundary fraction 0.5, vbar = 0.990 cm^3/g) as "vbar (full LNP)", 0.53 cm^3/g and 1.014 cm^3/g for the mRNA and lipid vbar, we obtain a composition of 95% lipid and thus 5% mRNA.

Deconvoluting the entire vbar distribution in this fashion (Fig. 4), we found the loaded LNP-1156 particles to consist of 92–96% lipid and conversely of 4–8% mRNA. A complete list of all values is provided in Table S1. These values can be applied to the molecular mass distribution

of the full particles also obtained from the density contrast experiment to arrive at molecular mass of the mRNA at each point of the molar mass distribution. By dividing these values though the molar mass of the mRNA (346 Da per base * 1156 bases = 400.000 Da/mol), we arrive at copy numbers per point. The resulting plot of copy number vs. sedimentation coefficient shows a discrete, stepwise distribution starting at a sedimentation coefficient of about 5 S and a copy number of 1 extending to an S-value of 50 and a copy number of 10. The weight average was found to be five copies per LNP. Quantifying the number of mRNAs per LNP with single particle imaging microscopy, Sabnis and co-workers (Sabnis et al. 2018) have found a weighted average of 4.6 of mRNAs/LNP with a size distribution like ours. Also, their poly-adenylated mCherry mRNA had a very similar size to our cargo (1010 vs 1156 nucleotides). Li and co-workers (Li et al. 2022) employed multi-laser cylindrical illumination confocal spectroscopy (CICS) to examine mRNA and lipid contents in LNP formulations at single-nanoparticle level. They determined a copy number of 2.8
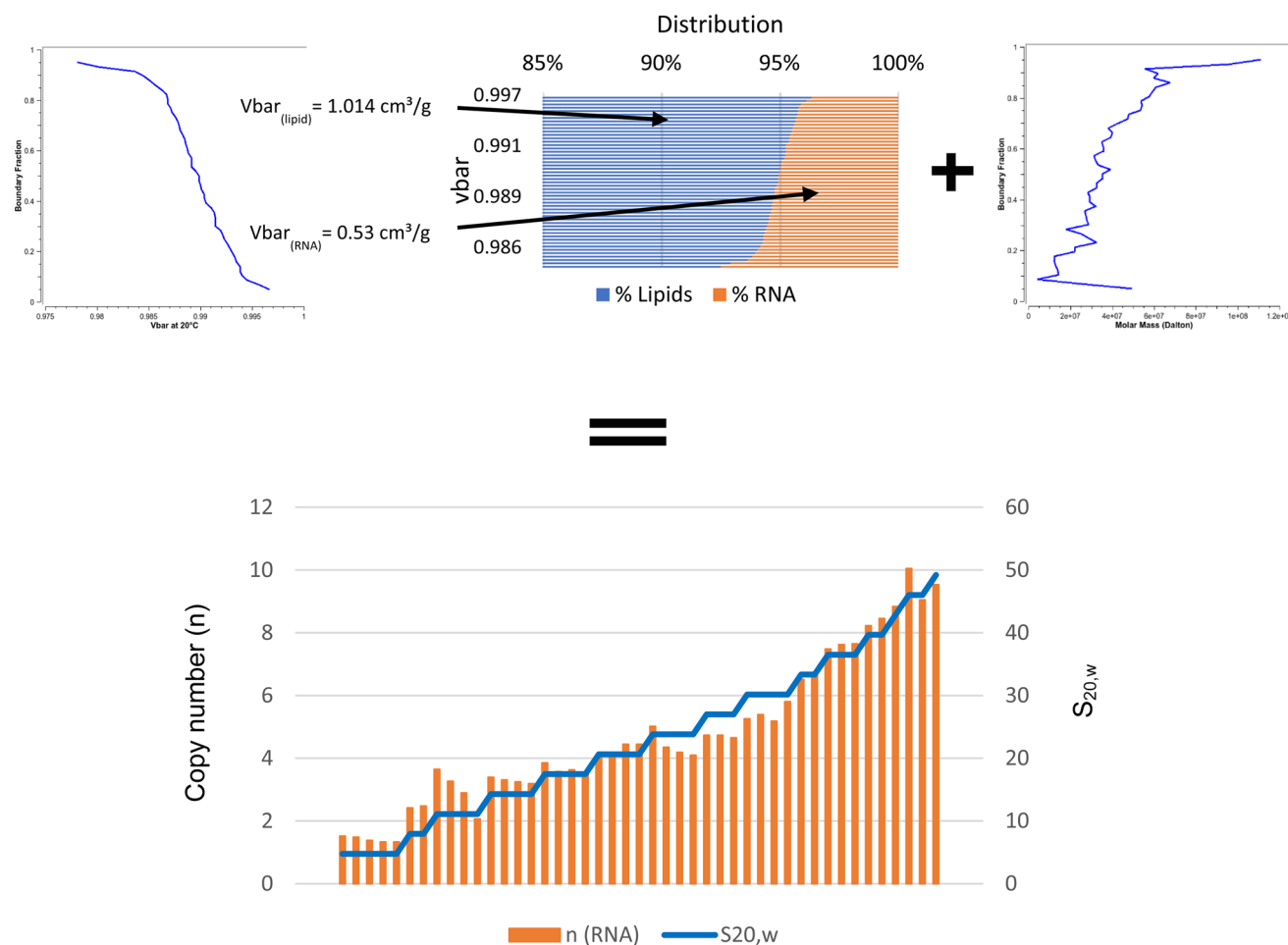
Fig. 4 Process flowchart of calculating copy numbers of RNA by deconvoluting molecular weight distribution into molecular weight (lipid) and molecular weight (RNA)

for their final formulation of a 1929-nt-long mRNA. The molar ratio of amine groups on ionizable lipids to phosphate groups on mRNA (N/P ratio) in their preparation was 6, while ours was 4.5. For an mRNA half of that size (852 nt), an average number of 26 VEGFa mRNAs per LNP has been found (Nawaz et al. 2023). The mRNA copy number for firefly luciferase mRNA was found to be proportional to volume of the LNP and inversely proportional to the N/P ratio resulting in one copy per LNP at an N/P ratio of 8 and 6 copies at an N/P ratio of 2 (Carrasco et al. 2021). Cui and colleagues were able to confirm that an increasing particle size is favorable for loading more mRNA copies per LNP, but the encapsulation efficiency was higher for smaller particles (Cui et al. 2022). The diameter of the LNPs under investigation in the studies cited above ranged from 40 to 100 nm. An investigation of larger LNPs with a diameter up to 200 nm by scattering techniques (SANS and SAXS) and cryo-electron microscopy (Yanez Arteta et al. 2018) revealed an exponential correlation between particle size and mRNA copy number. Starting with a diameter of 50 nm, the copy number for their 858-nt-long cargo ranged from 5 up to 200 mRNAs/LNP for LNPs with a diameter of 200 nm. Several hundreds of RNA molecules ($200-400$ copies) per LNP were so far only reported for much smaller siRNA (Kamanzi et al. 2021).

Using fluorescence correlation spectroscopy, Borodavka et al. (Borodavka et al. 2016) have found the hydrodynamic radius of 960-, 1200-, 1400-, and 1800 nt-long RNA molecules to be 8.8–11.9 nm. This concurs with AF4 (asymmetrical flow field-flow fractionation) measurements on single-stranded RNA molecules of 500–1800 nt length with hydrodynamic radii ranging from 8.4 to 14.7 nm (Eskelin et al. 2022). Considering the hydrodynamic radius of mRNAs and our LNP preparation (25–100 nm, Fig. 3E), a single-digit mRNA copy number as determined in this study as well as in the work of Sabnis, Li or Carrasco seems plausible. However, if mRNAs exist within solvent-filled cavities or may be substantially lipid associated as determined by contrast enhanced Cryo-EM (Brader et al. 2021) and given the r^3 dependency of the particle radius to its volume, these very large LNPs (200 nm) may provide a much higher distribution volume for mRNA molecules compared to smaller LNPs. Consequently, modulation of the particle size by control of the PEG-lipid concentration should enable direct control of the copy number for a given N/P ratio. An increasing concentration of PEG-lipid was shown to decrease the particle size (Ryals et al. 2020), while it also reduced the LNPs immunostimulatory potential and also hindered the in vivo efficacy (Kumar et al. 2014).

As for any other sedimentation velocity experiment, the reproducibility of the sedimentation coefficient distribution is crucial to assess the method performance. Figure S1 shows the size distribution of three independent experiments

as discrete distributions and as bar charts (sigma set to 0 in the "combine discrete species distributions" module of Ultrascan). They overlay well, but visual inspection lacks statistical confidence. The literature on this subject has been focused on the quantitation of trace amounts of aggregates in monodisperse therapeutic protein formulations, namely monoclonal antibodies (Gabrielson and Arthur 2011; Arthur et al. 2015). Overall, a precision of 0.5–1% for the quantitation of individual species and a reproducibility of 0.1 S or even better (especially for the intra-assay precision) for the S-values of the main species (monomer) has been found (Arthur et al. 2009; Gabrielson et al. 2010; Doyle et al. 2020).

To assess the reproducibility of our more complex s-value distribution, we determined the mean of the weight-average sedimentation coefficient, D10, D50, D90 and the span of three independent experiments (Table 1) of the full particles. The first data of the full particles (labeled "experiment 1" in Table 1) were gathered alongside with six D2O concentrations of the empty particles (Fig. 2). Experiment 2 was the D2O = 0 concentration from Fig. 3 and experiment 3 the 260 nm data from the multiwavelength run (Fig. S3A). We determined the mean of the weight-average sedimentation coefficient to be 22.3 S with a standard deviation of 0.8 S which is much higher than for a monodisperse system but in good agreement with the standard deviation found for a similar size distribution of Ferritin (17.0 ± 0.6 S, (May et al. 2010)), although our replicates were gathered over three independent experiments. The same precision was determined for the D50, while D10 and D90 varied to a higher degree due to the tailing of the distributions on both ends. The deviating values (especially D10 and D90) from experiment 3 compared to the other two runs are likely rooted in the lower data density and the late arrival of the first scan as it is only one dataset (260 nm) from a multiwavelength experiment (230–290 nm, 2 nm increment).

We also employed multiwavelength SV-AUC to examine the loading status of LNP-1156. Figure S2 shows the UV-absorbance spectra of the empty and full LNP samples, and the free mRNA obtained through lysis using TritonX-100.

Table 1 Selected size-distribution parameters from three independent SV-AUC experiments of the full LNPs

Experiment	1	2	3	Mean	Std dev
Total OD260	0.967	0.999	0.982	0.983	0.011
Mean (S20,w)	23.0	22.9	21.1	22.3	0.8
D10	3.7	2.9	−1.0	1.9	1.9
D50	22.1	21.7	20.2	21.3	0.8
D90	49.5	49.5	46.4	48.5	1.4
Span ((D90-D10)/D50)	2.1	2.1	2.4	2.2	0.1

The UV-spectra of both LNP preparations are dominated by the characteristic exponentially decaying light scattering signal as they do not contain a defined chromophore. The mRNA in LNP-1156 can be discerned as a shallow peak between 250 and 290 nm, while the free mRNA exhibits a maximum at 260 nm.

The MWL SV-AUC analysis of the empty LNPs confirmed the exponentially decaying light scattering pattern (higher intensity at shorter wavelengths) of the major species between −1 and −100 Svedberg (Fig. S3). The free mRNA around 5 S showed a maximum around 260 nm. The UV-spectrum of the smallest species of LNP-1156 at 5 S is dominated by a maximum around 240 nm and shows a decaying signal like the empty particles with a shallow shoulder at 260 nm. With increasing S-value, the signal at 260 nm is also increased until it is clearly dominating the species around 50 S. Therefore, we concluded that the loading status of LNP-1156 starts at a low copy number at 5 S (almost empty particles) and extends to multiple copy numbers (but not dozens or hundreds). In case the distribution would have ranged from for example 50 to 60 mRNA copies per LNP, the spectral composition of each peak would have changed only slightly. The data support the previous finding of a single-digit mRNA copy number per particle. Without knowing the Mie coefficients associated with the light scattering signal, we could not assign extinction coefficients to deconvolute the MWL sedimentation spectra further as outlined by Henrickson and co-workers. Attempts to assign arbitrary or relative signal increments to the empty LNPs did not result in a satisfactory quality of the signal deconvolution. Still, the MWL data provide visual evidence for the finding of only a few mRNA copies per particle.

Conclusion

Density contrast AUC offers a rapid and simple assay for the determination of mRNA copy numbers for lipid nanoparticle formulations. We have determined a discrete distribution ranging from 1 to 10 mRNA copies with an average of 5 copies per particle for our LNP formulation. However, potential users should keep two limitations in mind. First, this assay cannot distinguish between full length and degraded mRNA and thus confirm the integrity of the encapsulated nucleic acid. An LNP with 5 mRNA copies will have the same density as a particle with 10 half copies. This must be monitored by other assays such as (capillary) gel electrophoresis during drug substance/drug product characterization. Second, the data analysis assumes that the density and the ionic strength of the solvent inside the particle is the same as that of the bulk solvent. This may not be critical for dilute buffers like PBS but may become an issue in formulations containing high concentrations of excipients, especially salt as it may alter the vbar of the nucleic acid. A special attention should also be paid to the preparation of the D_2O containing buffer (D_2O is hygroscopic) as the low density of empty and full particles requires only a few percent of D_2O to match the density.

References

Arthur KK, Gabrielson JP, Kendrick BS, Stoner MR (2009) Detection of protein aggregates by sedimentation velocity analytical ultracentrifugation (SV-AUC): sources of variability and their relative importance. J Pharm Sci 98:3522–3539. https://doi.org/10.1002/jps.21654

Arthur KK, Kendrick BS, Gabrielson JP (2015) Guidance to achieve accurate aggregate quantitation in biopharmaceuticals by SV-AUC. Methods Enzymol 562:477–500

Bangham AD, Standish MM, Watkins JC (1965) Diffusion of univalent ions across the lamellae of swollen phospholipids. J Mol Biol 13:238-IN27. https://doi.org/10.1016/S0022-2836(65)80093-6

Bobo D, Robinson KJ, Islam J et al (2016) Nanoparticle-based medicines: a review of FDA-approved materials and clinical trials to date. Pharm Res 33:2373–2387. https://doi.org/10.1007/s11095-016-1958-5

Borodavka A, Singaram SW, Stockley PG et al (2016) Sizes of Long RNA molecules are determined by the branching patterns of their secondary structures. Biophys J 111:2077–2085. https://doi.org/10.1016/j.bpj.2016.10.014

Brader ML, Williams SJ, Banks JM et al (2021) Encapsulation state of messenger RNA inside lipid nanoparticles. Biophys J 120:2766–2770. https://doi.org/10.1016/j.bpj.2021.03.012

Carrasco MJ, Alishetty S, Alameh M-G et al (2021) Ionization and structural properties of mRNA lipid nanoparticles influence expression in intramuscular and intravascular administration. Commun Biol 4:956. https://doi.org/10.1038/s42003-021-02441-2

Cui L, Hunter MR, Sonzini S et al (2022) Mechanistic studies of an automated lipid nanoparticle reveal critical pharmaceutical properties associated with enhanced mRNA functional delivery in vitro and in vivo. Small 18:2105832. https://doi.org/10.1002/smll.202105832

Demeler B, Gorbet GE (2016) Analytical ultracentrifugation data analysis with ultrascan-III. Analytical ultracentrifugation. Springer Japan, Tokyo, pp 119–143

Doyle BL, Rauk AP, Weiss WF, Budyak IL (2020) Quantitation of soluble aggregates by sedimentation velocity analytical ultracentrifugation using an optical alignment system–Aspects of method validation. Anal Biochem 605:113837. https://doi.org/10.1016/j.ab.2020.113837

Enger MD, Stubbs EA, Mitra S, Kaesberg P (1963) BIOPHYSICAL CHARACTERISTICS OF THE RNA-CONTAINING BACTERIAL VIRUS R17. Proc Natl Acad Sci 49:857–860. https://doi.org/10.1073/pnas.49.6.857

Eskelin K, Lampi M, Coustau C et al (2022) Analysis and purification of ssRNA and dsRNA molecules using asymmetrical flow field flow

fractionation. J Chromatogr A 1683:463525. https://doi.org/10.1016/j.chroma.2022.463525

Funari SS, Rapp G, Perbandt M et al (2000) Structure of Free Thermus flavus 5 S rRNA at 1.3 nm resolution from synchrotron X-ray solution scattering. J Biol Chem 275:31283–31288. https://doi.org/10.1074/jbc.M004974200

Gabrielson JP, Arthur KK (2011) Measuring low levels of protein aggregation by sedimentation velocity. Methods 54:83–91. https://doi.org/10.1016/j.ymeth.2010.12.030

Gabrielson JP, Arthur KK, Stoner MR et al (2010) Precision of protein aggregation measurements by sedimentation velocity analytical ultracentrifugation in biopharmaceutical applications. Anal Biochem 396:231–241. https://doi.org/10.1016/j.ab.2009.09.036

Gorbet GE, Pearson JZ, Demeler AK et al (2015) Next-Generation AUC: analysis of multiwavelength analytical ultracentrifugation data. Methods in enzymology. Academic Press Inc., Cambridge, pp 27–47

Hayes DB, Dobnik D (2022) Commentary: multiplex dPCR and SV-AUC are promising assays to robustly monitor the critical quality attribute of AAV drug product integrity. J Pharm Sci 111:2143–2148. https://doi.org/10.1016/j.xphs.2022.04.010

Hayes DB, Philo JP, Laue TM (2000) SedNTerp: interpretation of sedimentation data

Henrickson A, Kulkarni JA, Zaifman J et al (2021) Density matching multi-wavelength analytical ultracentrifugation to measure drug loading of lipid nanoparticle formulations. ACS Nano 15:5068–5076. https://doi.org/10.1021/acsnano.0c10069

Henrickson A, Gorbet GE, Savelyev A et al (2022) Multi-wavelength analytical ultracentrifugation of biopolymer mixtures and interactions. Anal Biochem 652:114728

Horne CR, Henrickson A, Demeler B, Dobson RCJ (2020) Multi-wavelength analytical ultracentrifugation as a tool to characterize protein–DNA interactions in solution. Eur Biophys J 49:819–827. https://doi.org/10.1007/s00249-020-01481-6

Kamanzi A, Gu Y, Tahvildari R et al (2021) Simultaneous, single-particle measurements of size and loading give insights into the structure of drug-delivery nanoparticles. ACS Nano 15:19244–19255. https://doi.org/10.1021/acsnano.1c04862

Kumar V, Qin J, Jiang Y et al (2014) Shielding of Lipid Nanoparticles for siRNA Delivery: Impact on Physicochemical Properties, Cytokine Induction, and Efficacy. Mol Ther Nucleic Acids 3:e210. https://doi.org/10.1038/mtna.2014.61

Laue TM, Shah BD, Ridgeway TM, Pelletier SL (1992) Computer-Aided Interpretation of analytical sedimentation data for proteins. In: Harding SE, Rowe AJ, Horton JC (eds) Analyical Ultracentrifugation in Biochemistry and Polymer Sciences. Royal Society of Chemistry, London, pp 90–125

Li S, Hu Y, Li A et al (2022) Payload distribution and capacity of mRNA lipid nanoparticles. Nat Commun 13:5561. https://doi.org/10.1038/s41467-022-33157-4

Malone RW, Felgner PL, Verma IM (1989) Cationic liposome-mediated RNA transfection. Proc Natl Acad Sci 86:6077–6081. https://doi.org/10.1073/pnas.86.16.6077

Marquis BJ, Love SA, Braun KL, Haynes CL (2009) Analytical methods to assess nanoparticle toxicity. Analyst 134:425. https://doi.org/10.1039/b818082b

Maruno T, Usami K, Ishii K et al (2021) Comprehensive size distribution and composition analysis of adeno-associated virus vector by multiwavelength sedimentation velocity analytical ultracentrifugation. J Pharm Sci 110:3375–3384. https://doi.org/10.1016/j.xphs.2021.06.031

Maruno T, Ishii K, Torisu T, Uchiyama S (2022) Size distribution analysis of the adeno-associated virus vector by the c(s) analysis of band sedimentation analytical ultracentrifugation with multiwavelength detection. J Pharm Sci. https://doi.org/10.1016/j.xphs.2022.10.023

May CA, Grady JK, Laue TM et al (2010) The sedimentation properties of ferritins. New insights and analysis of methods of nanoparticle

preparation. Biochimica et Biophysica Acta 1800:858–870. https://doi.org/10.1016/j.bbagen.2010.03.012

McIntosh NL, Berguig GY, Karim OA et al (2021) Comprehensive characterization and quantification of adeno associated vectors by size exclusion chromatography and multi angle light scattering. Sci Rep 11:3012. https://doi.org/10.1038/s41598-021-82599-1

Nawaz M, Heydarkhan-Hagvall S, Tangruksa B et al (2023) Lipid nanoparticles deliver the therapeutic VEGFA mRNA in vitro and in vivo and transform extracellular vesicles for their functional extensions. Adv Sci. https://doi.org/10.1002/advs.202206187

Padlan CS, Malashkevich VN, Almo SC et al (2014) An RNA aptamer possessing a novel monovalent cation-mediated fold inhibits lysozyme catalysis by inhibiting the binding of long natural substrates. RNA 20:447–461. https://doi.org/10.1261/rna.043034.113

Philo JS (2023) SEDNTERP: a calculation and database utility to aid interpretation of analytical ultracentrifugation and light scattering data. Eur Biophys J. https://doi.org/10.1007/s00249-023-01629-0

Ramachandran S, Satapathy SR, Dutta T (2022) Delivery strategies for mRNA vaccines. Pharmaceut Med 36:11–20. https://doi.org/10.1007/s40290-021-00417-5

Ryals RC, Patel S, Acosta C et al (2020) The effects of PEGylation on LNP based mRNA delivery to the eye. PLoS One 15:e0241006. https://doi.org/10.1371/journal.pone.0241006

Sabnis S, Kumarasinghe ES, Salerno T et al (2018) A novel amino lipid series for mRNA delivery: improved endosomal escape and sustained pharmacology and safety in non-human primates. Mol Ther 26:1509–1519. https://doi.org/10.1016/j.ymthe.2018.03.010

Tenchov R, Bird R, Curtze AE, Zhou Q (2021) Lipid Nanoparticles─From Liposomes to mRNA vaccine delivery, a landscape of research diversity and advancement. ACS Nano 15:16982–17015. https://doi.org/10.1021/acsnano.1c04996

Thaller A, Schmauder L, Frieß W et al (2023) SV-AUC as a stability-indicating method for the characterization of mRNA-LNPs. Eur J Pharm Biopharm 182:152–156. https://doi.org/10.1016/j.ejpb.2022.11.014

Voss NR, Gerstein M (2005) Calculation of standard atomic volumes for RNA and comparison with proteins: RNA is packed more tightly. J Mol Biol 346:477–492. https://doi.org/10.1016/j.jmb.2004.11.072

Walter J, Sherwood PJ, Lin W et al (2015) Simultaneous analysis of hydrodynamic and optical properties using analytical ultracentrifugation equipped with multiwavelength detection. Anal Chem 87:3396–3403. https://doi.org/10.1021/ac504649c

Wilson SC, Baryza JL, Reynolds AJ et al (2015) Real time measurement of PEG shedding from lipid nanoparticles in serum via NMR spectroscopy. Mol Pharm 12:386–392. https://doi.org/10.1021/mp500400k

Xia T, Kovochich M, Brant J et al (2006) Comparison of the abilities of ambient and manufactured nanoparticles to induce cellular toxicity according to an oxidative stress paradigm. Nano Lett 6:1794–1807. https://doi.org/10.1021/nl061025k

Yanez Arteta M, Kjellman T, Bartesaghi S et al (2018) Successful reprogramming of cellular protein production through mRNA delivered by functionalized lipid nanoparticles. Proc Natl Acad Sci. https://doi.org/10.1073/pnas.1720542115

Yin H, Kanasty RL, Eltoukhy AA et al (2014) Non-viral vectors for gene-based therapy. Nat Rev Genet 15:541–555. https://doi.org/10.1038/nrg3763